Lawrence Berkeley National Laboratory

Title

Surfactant-Induced Interfacial Aggregation of Porphyrins for Structuring Color-Tunable
Liquids

Authors

Gu, Pei-Yang
Xie, Ganhua
Kim, Paul Y
et al.

Surfactant-induced interfacial aggregation of porphyrins for structuring the color-tunable liquids

Pei-Yang Gu,[a, b] Ganhua Xie,[b] Paul Y. Kim,[b] Yu Chai,[b, c] Xuefei Wu,[b, f] Yufeng Jiang,[b] Qing-Feng Xu,[a] Feng Liu,[d] Jian-Mei Lu*[a] and Thomas P. Russell*[b, e, f]

Communications

Abstract: Locking-in nonequilibrium shapes of liquids into targeted architectures by the interfacial jamming of nanoparticles, i.e. structuring liquids, is an emerging area in material science. Here, 5,10,15,20-tetrakis(4-sulfonatophenyl) porphyrin (H_6TPPS) shows three different aggregation states that present an absorption imaging platform to monitor the assembly and jamming of nanoparticle surfactants at the liquid/liquid interface. The interfacial interconversion of H_6TPPS, specifically H_4TPPS^{2-} dissolved in water, from a J to an H-aggregation state was induced by strong electrostatic interactions with amine terminated polystyrene dissolved in toluene at the water/toluene interface. This resulted in color-tunable liquids due to interfacial jamming of the supramolecular polymer surfactants formed between H_4TPPS^{2-} and amine terminated polystyrene. However, the supramolecular polymer surfactants formed cannot lock-in nonequilibrium shapes of liquids. In addition, a self-wrinkling behavior was observed when amphiphilic triblock copolymers of PS-*block*-poly(2-vinylpyridine)-*block*-poly(ethylene oxide) were used to interact with H_4TPPS^{2-}. Subsequently, the supramolecular polymer surfactants formed can lock-in nonequilibrium shapes of liquids. The interfacial assembly and chromogenic transitions of these aggregates provided the optical insights into the formation, assembly and jamming of supramolecular polymer surfactants and the structuring of liquids.

Controlling the aggregation of organic molecules by non-covalent intermolecular interactions to form supramolecular structures provides an avenue to mimic natural systems, since they afford a triggering mechanism for responsive supramolecular structures, and have potential technological applications due to their optoelectronic properties.[1-4] Correspondingly, porphyrin aggregates play important roles in photosynthetic and photocatalytic systems.[5-8] As a model system, 5,10,15,20-tetrakis(4-sulfonatophenyl) porphyrin (H_6TPPS, Scheme S1) shows three different aggregation states with disparate optoelectronic properties, including J- and H-aggregates of the diacid form (H_4TPPS^{2-}, Scheme 1) and an H-aggregate of free-base form (H_2TPPS^{4-}, Scheme 1).[9-14] A transition from a J- to an H-aggregate of H_4TPPS^{2-} to an H-aggregate of H_2TPPS^{4-} can be induced and controlled by changes in concentration, pH, ionic strength, or temperature, the presence of polyelectrolytes in the bulk or at solid/liquid interfaces. However, the transition of H_4TPPS^{2-} at a liquid/liquid interface, specifically the water/oil interface, is mostly unexplored. Liquid/liquid interfaces afford some unique opportunities, due to the ease of chemical manipulation of the supramolecular structures, the interfacial assemblies are highly mobile, rapidly achieving equilibrium, the reaction behavior at the interface differs from that in the bulk, and H_4TPPS^{2-} can electrostatically interact with basic hydrophobic polymers or oligomers to form supramolecular polymer surfactants (SPSs) where the interfacial binding energy is significantly increased, enabling the structuring of the liquids by an interfacial jamming.[15-23]

Recently, locking-in non-equilibrium shapes of liquids into targeted architectures, i.e. structuring the liquids, using the interfacial assembly and jamming of nanoparticles, is emerging as a strategy for encapsulation for delivery systems to bicontinuous all-liquid systems for electron and ion transduction to separations for energy generation and storage devices to all-liquid, adaptable and responsive, three-dimensional (3D) printed constructs.[24–32] While the components comprising these "structured liquids" can integrate their own inherent functionality, the jamming of nanoparticles at the interface can transform the fundamental nature of the assemblies, as demonstrated with the recent discovery of ferromagnetic liquid droplets where magnetic nanoparticles are used.[33] Chromogenic materials open further opportunities to generate responsive all-liquid constructs that can act as sensory devices but also provide unique opportunities to gain fundamental insights into assemblies of the nanoparticles at the fluid interface that form the basis for structuring the liquids.[34-41]

One such chromogenic material is H_6TPPS, since the optical properties of H_6TPPS can be altered by controlling the aggregation at the liquid/liquid interface.

[a]   Dr. P.-Y. Gu, Prof. Q.-F. Xu, Prof. J.-M. Lu
        College of Chemistry, Chemical Engineering and Materials
        Science, Collaborative Innovation, Center of Suzhou Nano
        Science and Technology, Soochow University, Suzhou,
        215123, China.
        E-mail: lujm@suda.edu.cn
[b]   Dr P.-Y. Gu, Dr Y. Chai, Dr. G. Xie, Y. Jiang, Prof. T. P. Russell
        Materials Sciences Division, Lawrence Berkeley National
        Laboratory, 1 Cyclotron Road, Berkeley, CA 94720 (USA)
        E-mail: russell@mail.pse.umass.edu
[c]   Dr Y. Chai
        Molecular Foundry, Lawrence Berkeley National Laboratory,
        1 Cyclotron Road, Berkeley, CA 94720 (USA)
[d]   Dr. F. Liu
        Department of Physics and Astronomy, Collaborative
        Innovation Center of IFSA (CICIFSA), Shanghai Jiaotong
        University, Shanghai 200240, P. R. China.
[e]   Prof. T. P. Russell
        Polymer Science and Engineering Department, University of
        Massachusetts, Amherst, MA 01003 (USA)
[f]   Prof. T. P. Russell
        Beijing Advanced Innovation Center for Soft Matter Science
        and Engineering, Beijing University of Chemical Technology,
        Beijing 100029, China
        Supporting information for this article is given via a link at

We investigated the interfacial assembly of H_6TPPS as a function of the number and alkalinity of functionalized polymers that anchor to the H_6TPPS to understand the relationship between aggregation states and structuring the liquids. As shown in Scheme S1, as a strong acid, H_6TPPS produces protons in water to form a negative ion H_4TPPS^{2-}. Four different functionalized hydrophobic polymer architectures with increasing interfacial reactivity (Scheme 1), including end-functionalized and multi-functional homopolymers and triblock copolymers, were investigated to understand the role of the alkalinity, hydrophilicity and hydrophobicity of the anchored polymers in inducing conversion of H_4TPPS^{2-} at the water/oil interface and structuring the colorable liquids (Scheme 1). First, electrostatic interactions between H_4TPPS^{2-} and amino terminated polystyrene (PS-NH$_2$) were investigated. Second, the influence of alkalinity and hydrophilicity was then examined using ω-(diethylene triamine)-terminated polystyrene (PS-triNH$_2$) for comparison with PS-NH$_2$ because PS-triNH$_2$ has three amino groups. Third, the formation of SPSs with multifunctional polymers poly(2-vinylpyridine) (P2VP) was investigated since the assemblies and jamming are more quickly due to the multiple 2VP sites along the chain. Fourth, triblock copolymers of PS-*block*-P2VP-*block*-poly(ethylene oxide) (PS-*b*-P2VP-*b*-PEO) was investigated, since the assemblies are further fast and stabilized by an effective crosslinking of the triblock copolymer chains at the interface (Scheme S2). The stability of jamming could be influenced by the anchoring to a polymer chain, and the surfactant nature of polymer with the functionality on the backbone of the polymer can be different than that of end-functionalized chains and homopolymers.
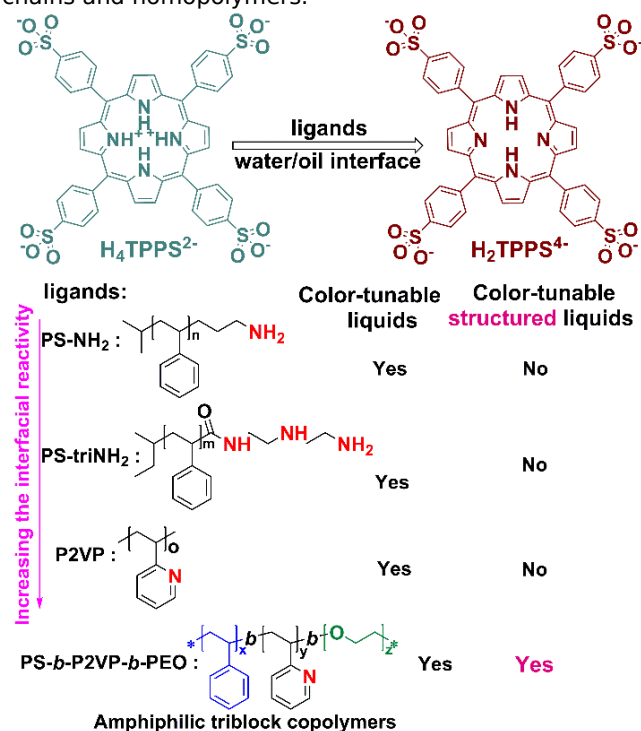
Scheme 1. H_4TPPS^{2-} can be induced to H_4TPPS^{2-} by interactions with alkalinity ligands at the water/oil interface.

Figure 1a shows the color change of a water droplet containing H_4TPPS^{2-} (0.4 g L^{-1}, pH = 3.4) as a function of time and concentration of PS-NH$_2$ in toluene solutions. For low PS-NH$_2$ concentrations (from 0 to 0.05 g L^{-1}), no obvious color change is observed. At a moderate PS-NH$_2$ concentration (0.1 g L^{-1}), the color of the interface between the water droplet and toluene solution changes from green to light red with time, indicating that some of H_4TPPS^{2-} has interacted with the PS-NH$_2$ to form SPSs that have aggregated at the interface. At a high PS-NH$_2$ concentrations (>0.5 g L^{-1}), the color of the water droplet surface immediately changes to light red and, gradually, the entire droplet undergoes this color change, due to a depletion of H_4TPPS^{2-} in the water droplet. At higher PS-NH$_2$ concentrations (from 1.0 to 10 g L^{-1}), the color of the entire droplet changes from green to light red after 30 minutes, and for PS-NH$_2$ concentrations >10 g L^{-1}, the droplet is colorless after 120 minutes, since most, if not all, of the H_4TPPS^{2-} has assembled at the water/toluene interface. The observed color changes have their origins in the transition of J-aggregates (green) to H-aggregates (light red) of H_4TPPS^{2-}. The UV-visible absorption spectra of the interfacial films were measured (Figure 1b). When a concentration of PS-NH$_2$ is 0.05 g L^{-1}, a sharp Soret absorption band at 490 nm and Q-bands at 633 and 706 nm are observed, that arise from J-aggregates of H_4TPPS^{2-}, along with a weak Soret absorption band at 424 nm, associated with H-aggregates of H_4TPPS^{2-}. The intensity of the Soret band at 424 nm increases and at 490 nm decreases with increasing concentration of PS-NH$_2$, indicating that, with increasing PS-NH$_2$, the J-type of porphyrin has transitioned to an H-aggregate of H_4TPPS^{2-}. When the concentration of PS-NH$_2$ increases to 0.5 g L^{-1}, new Q-bands at 521, 557, 596 and 650 nm appear. At a higher PS-NH$_2$ concentration (1.0 g L^{-1}), the Q-band at 706 nm virtually disappears. When the concentration of PS-NH$_2$ is increased to 10.0 g L^{-1}, the Soret band at 490 nm and the Q-band at 706 nm vanish. As revealed in Figure S6-S13, the interaction between PS-NH$_2$ and H_4TPPS^{2-} in solution can lead to the conversion from H_4TPPS^{2-} to H_2TPPS^{4-}. However, such behavior cannot be observed by the interfacial assembly because the SPSs formed films may block the further interaction between new porphyrin molecules and PS-NH$_3^+$. The interactions between the H_4TPPS^{2-} and the PS-NH$_3^+$ result in the formation of SPSs where multiple PS-NH$_3^+$ interact with H_4TPPS^{2-}. The strong interfacial binding can give rise to jamming and wrinkling of SPSs, when the interfacial area is decreased.[42] For a pendant drop, the ratio of the volume at which wrinkling is observed to the initial volume, V_w/V_i, provides a rough estimate of the initial coverage of the interface. As shown in Figure 1c and Figure S14, at PS-NH$_2$ concentrations from 0 to 0.1 g L^{-1}, V_w/V_i increases with increasing PS-NH$_2$ concentration. At a PS-NH$_2$ concentration of 0.01 g L^{-1}, V_w/V_i is ~0.16. When the concentration of PS-NH$_2$ increases to 0.1 g L^{-1}, V_w/V_i is ~0.95. However, V_w/V_i dramatically decreases with a further increase in PS-NH$_2$ concentration. At the PS-NH$_2$ concentration of 0.2 g L^{-1}, V_w/V_i is only ~0.02, and no obvious wrinkling is observed for higher PS-NH$_2$

concentrations, but films formation is evident, with the film peeling away from the interface (Figure S14). This demonstrates that a film is formed but the assembly appears to be rigid, so much so that this film does not winkle but, rather, is broken-up into smaller sheets that are pushed on top of one another, leading to a slipping of one sheet over the other and eventually a removal of these strips from the interface as the interfacial area is decreased. Consequently, the number of SPSs formed increases with increasing PS-NH$_2$ concentration and color-tunable liquids can be achieved, but the SPSs formed between H$_4$TPPS^{2-} and high PS-NH$_2$ concentration (above a concentration of 0.2 g L^{-1}) cannot lock-in nonequilibrium shapes of liquids (V_w/V_i is only ~0.02). As shown in Figure S15/S16, PS-NH$_2$ shows the interfacial activity but PS-NH$_2$ does not wrinkle because the binding energy of per PS-NH$_2$ is not sufficient to withstand compression as the liquids attempt to return to their equilibrium shape.
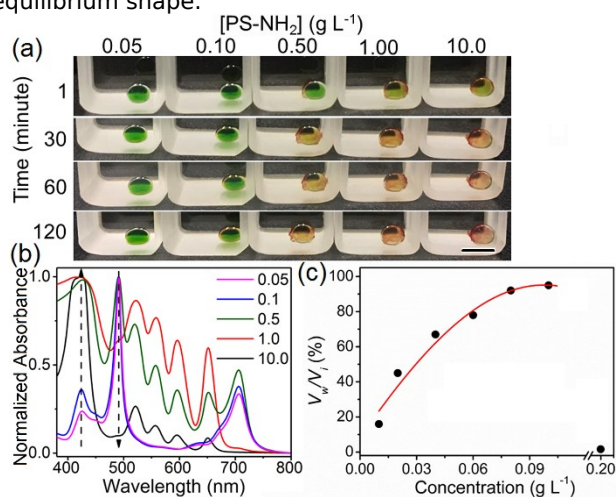

Figure 1. (a) Color change of H$_4$TPPS^{2-} (0.4 g L^{-1}, pH = 3.4) in water against PS-NH$_2$ in toluene solution at different concentration and different time. Scale bar: 0.5 cm. (b) The UV-visible absorption spectra of interface films between water/H$_4$TPPS^{2-} and toluene/PS-NH$_2$. (c) Compression ratio of 30 minutes aged water droplets as a function of the PS-NH$_2$ concentration.

With PS-NH$_2$, PS-triNH$_2$, and P2VP in toluene, the formed SPSs with H$_4$TPPS^{2-} are stable against compression at low polymer concentrations and can be used to structure liquids. However, at higher polymer concentrations, multilayers of SPSs form, making the films unstable to compression, leading that the formed SPSs cannot lock-in nonequilibrium shapes of liquids. Consequently, the interactions between H$_4$TPPS^{2-} and triblock copolymers of PS-b-P2VP-b-PEO were investigated, since the interactions of the H$_4$TPPS^{2-} with the P2VP is mediated by the presence of the PS and PEO block because the PS (a hydrophobic polymer) and PEO (a hydrophilic polymer) can be used to balance changes in polymer chain polarity. Figure 2a shows the color change of a water droplet containing H$_4$TPPS^{2-} (0.4 g L^{-1}, pH = 3.4) as a function of time and concentration of PS-b-P2VP-b-PEO in toluene. For low PS-b-P2VP-b-PEO concentrations (from 0 to 0.05 g L^{-1}), no obvious color change is observed over time. This behavior is similar to

that for PS-NH$_2$, PS-triNH$_2$, and P2VP. However, the shapes of the droplets change from spherical to oblate ellipsoidal, indicating a further reduction in the interfacial energy and the formation of SPS-like species at the interface. Also, the contact angle continually decreases as the concentration of PS-b-P2VP-b-PEO increases, since more SPSs are formed at the interface. Unlike PS-NH$_2$, PS-triNH$_2$, and P2VP, though, at PS-b-P2VP-b-PEO concentration as high as 2.00 g L^{-1}, the color of the water droplet changes from green to red and the interface films are stable. The thickness of the film increases with increasing PS-b-P2VP-b-PEO concentration, but the SPSs formation at the interface is stable, suggesting that the SPSs formation can lock-in nonequilibrium shapes of liquids into targeted architectures, no matter what the aggregate state of the porphyrin and the concentration of ligands. Figure 2b shows the UV-visible absorption spectra of the interfacial films between H$_4$TPPS^{2-} and PS-b-P2VP-b-PEO at the water/toluene interface. When the concentration of PS-b-P2VP-b-PEO is 0.05 g L^{-1}, Soret absorption bands at 422 nm (H-aggregates of H$_4$TPPS^{2-}) and 490 nm (J-aggregates of H$_4$TPPS^{2-}), and Q-bands at 633 and 707 nm are seen. When the concentration of PS-b-P2VP-b-PEO is increased, the intensity of Soret band at 422 nm increases and the intensity of Soret band at 490 nm and Q-bands at 633 and 707 nm decrease, along with new Q-bands at 521, 557, 596 and 650 nm appears, indicating that J-type of porphyrin has changed to the H-aggregate of H$_4$TPPS^{2-} with the increase in concentration of PS-b-P2VP-b-PEO. At a high PS-b-P2VP-b-PEO concentration (5.0 g L^{-1}), the Soret bands at 490 and Q-band at 707 nm almost disappear, along with the appearance of a new Q-band at 407 nm, suggesting the formation of H-aggregates of H$_2$TPPS^{4-}. It is interesting to note that, when the concentration of PS-b-P2VP-b-PEO is 0.01 g L^{-1}, a self-wrinkling of the droplet is observed after aging for 500 s, due to the strong interactions between PS-b-P2VP-b-PEO and H$_4$TPPS^{2-} (Figure S23). By increasing the concentration of PS-b-P2VP-b-PEO, the self-wrinkling behavior is more evident. When the concentration of PS-b-P2VP-b-PEO increases to 5.0 g L^{-1}, self-wrinkling occurs after only 10 s, suggesting that H$_4$TPPS^{2-} may be used in print 3D structures according to our previous reports.[43,44] Using this method, it is easy to lock nonequilibrium shapes of the fluids into targeted architectures at the two fluids interface and it is also easy to observe the color change at the water/oil interface. Noting that PS-b-P2VP-b-PEO can dramatically lower the γ but PS-b-P2VP-b-PEO does not wrinkle because the binding energy of per PS-b-P2VP-b-PEO is not sufficient to withstand compression as the liquids attempt to return to their equilibrium shape, as show in Figure S15/S16/S25.
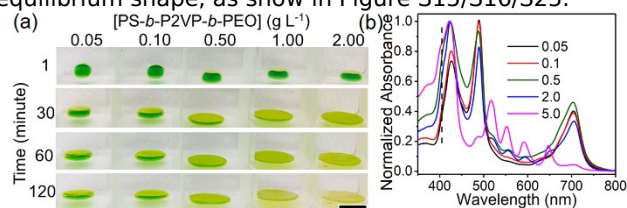

Figure 2. (a) Color change of H$_4$TPPS^{2-} (0.4 g L^{-1}, pH = 3.4) in water against PS-b-P2VP-b-PEO in toluene solution at different

concentration (g L^{-1}) and different time. Scale bar: 0.5 cm. (b) The UV-visible absorption spectra of interface films between water/ H$_4$TPPS^{2-} and toluene/ PS-*b*-P2VP-*b*-PEO.

To investigate the importance of balancing changes in polymer chain polarity on structuring liquids, another triblockcopolymer PS-*b*-P2VP-*b*-PEO (3200-*b*-1300-*b*-18000 g mol$^{-1,}$ named as PS-*b*-P2VP-*b*-PEO18k) containing a longer hydrophilic fragment was studied. As shown in Figure 3a/3b and Figure S26/S27, γ for different molecular weights of PS-*b*-P2VP-*b*-PEO (3200-*b*-1300-*b*-3000 and 3200-*b*-1300-*b*-18000, g mol^{-1}) was found to slightly decrease with increasing molecular weights due to lower diffusion coefficient of the longer PEO chains but V_w/V_i is totally different. As shown in Figure 3b and Figure S28/Figure S29, when the concentration of low molecular weight PS-*b*-P2VP-*b*-PEO (3200-*b*-1300-*b*-3000, g mol^{-1}) is increased to 0.5 μmol L^{-1}, V_w/V_i is ~1.00, much larger than high molecular weight PS-*b*-P2VP-*b*-PEO18k (3200-*b*-1300-*b*-18000, g mol^{-1}) (0.10), indicating that the molecular weights affect the stability of the liquid. For low molecular weight PS-*b*-P2VP-*b*-PEO (3200-*b*-1300-*b*-3000, g mol^{-1}), in high concentration (5.0 μmol L^{-1}), the self-wrinkling behavior can be observed, as show in Figure 3c. However, for high molecular weight PS-*b*-P2VP-*b*-PEO18k (3200-*b*-1300-*b*-18000, g mol^{-1}), in high concentration (5.0 μmol L^{-1}), some aggregates can be observed since the longer the PEO chain, the better the hydrophilicity of the triblockcopolymer, leading that the PS and PEO cannot efficiently balance changes in polymer chain polarity. Through the study of different molecular weights of triblockcopolymer, it is further proved that adjusting the hydrophilicity and hydrophobicity of the polymer chain is crucial to the stability of the SPSs at the interface.

Figure 4a/4b shows the UV-vis absorption results of the aqueous H$_4$TPPS^{2-} (0.4 g L^{-1}, pH = 3.4) in contact with a PS-NH$_2$ or PS-*b*-P2VP-*b*-PEO (5.0 g L^{-1}) solution in 1,2,4-trimethylbenzene. As shown in Figure S30, the top of the 1,2,4-trimethylbenzene phase was used for the UV-vis absorption measurement. For PS-NH$_2$, Soret absorption bands at 413 nm (monomer of H$_2$TPPS^{4-}) and 420 nm (H-aggregates of H$_4$TPPS^{2-}), and Q-bands at 520, 556, 595 and 650 nm are easy to observe after 30 s, suggesting that the SPSs formed by PS-NH$_2$ cannot stabilize at the 1,2,4-trimethylbenzene/water interface at the high concentration of PS-NH$_2$. Furthermore, the absorption intensity increases with increasing time. However, there is no obvious absorption peaks for PS-*b*-P2VP-*b*-PEO over time, indicating that the SPSs s formed by PS-*b*-P2VP-*b*-PEO can be stabilized at the 1,2,4-trimethylbenzene/water interface at the high concentration of PS-*b*-P2VP-*b*-PEO. Additionally, diffusion at the interface could be directly visualized by laser scanning fluorescence confocal microscopy (LSFCM). As shown in Figure 4c/d and Figure S31, when a water droplet containing H$_4$TPPS^{2-} is placed in a solution of PS-NH$_2$ in 1,2,4-trimethylbenzene, a red interface can be observed. Furthermore, a red color appears in the 1,2,4-trimethylbenzene phase and no obvious color observes in the water phase after 200 s because H$_4$TPPS^{2-} is transferred from the aqueous phase into water/oil interface to form SPSs which are being drawn away from the interface and into the 1,2,4-trimethylbenzene phase. However, for PS-*b*-P2VP-*b*-PEO, no obvious color appears in the 1,2,4-trimethylbenzene phase (Figure 4e/4f and Figure S32), indicating that the SPSs formed by PS-*b*-P2VP-*b*-PEO can be stabilized at the 1,2,4-trimethylbenzene/water interface even if at a high concentration of PS-*b*-P2VP-*b*-PEO, since the PS (a hydrophobic polymer) and PEO (a hydrophilic polymer) can be used to balance changes in polymer chain polarity.
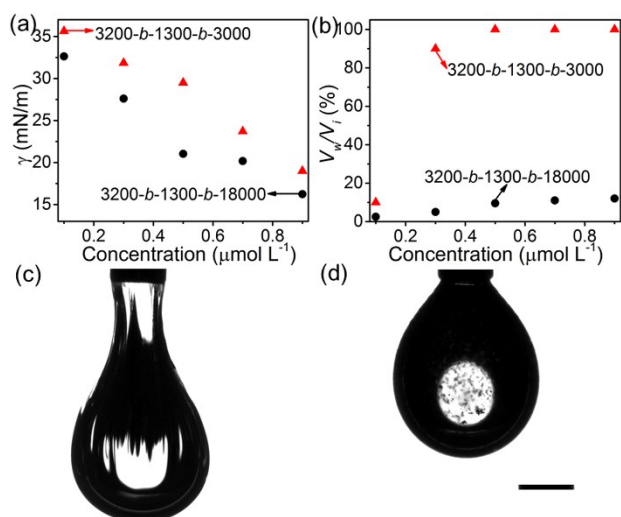

Figure 3. (a) Interfacial tension of H$_4$TPPS^{2-} (0.2 g L^{-1}, pH = 3.5) in water against different molecular weights PS-*b*-P2VP-*b*-PEO (3200-*b*-1300-*b*-3000 and 3200-*b*-1300-*b*-18000, g mol^{-1}) in toluene solution at different concentration. (b) Compression ratio of 30 minutes aged water droplets as a function of the PS-*b*-P2VP-*b*-PEO concentration. (c, d) A water droplet containing H$_4$TPPS^{2-} (0.2 g L^{-1}, pH = 3.5) against different molecular weights PS-*b*-P2VP-*b*-PEO ((c) 3200-*b*-1300-*b*-3000 and (d) 3200-*b*-1300-*b*-18000 g mol^{-1}, 5 μmol L^{-1}) in toluene solution after 30 minutes. Scale bar: 1.27 mm.
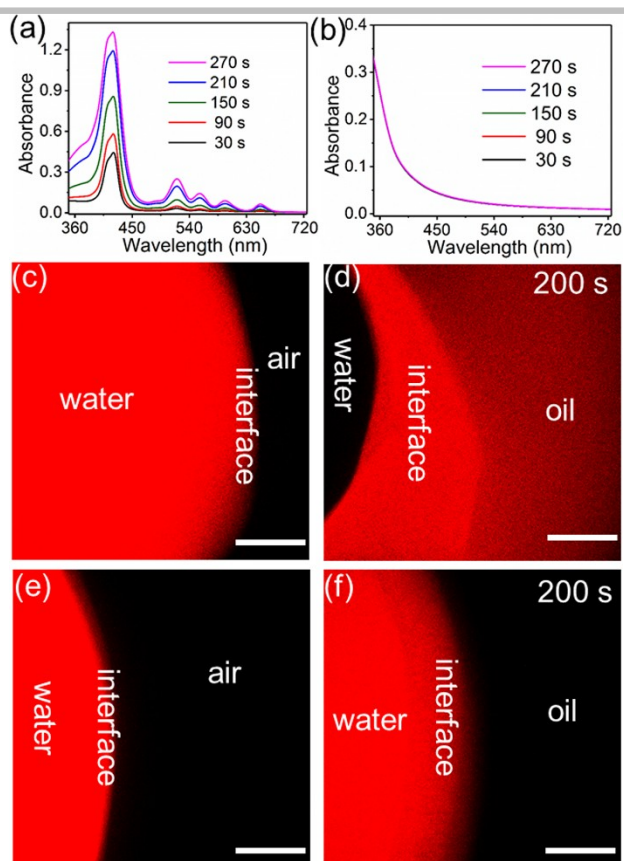
Figure 4 □ (a) The UV-visible absorption spectra of oil phase (the aqueous H_4TPPS^{2-} solution in contact with a PS-NH$_2$ solution in 1,2,4-trimethylbenzene). (b) The UV-visible absorption spectra of oil phase (the aqueous H_4TPPS^{2-} solution in contact with a PS-*b*-P2VP-*b*-PEO solution in 1,2,4-trimethylbenzene) (c, d) Confocal fluorescence microscopy images of a water droplet containing H_4TPPS^{2-} (0.4 g L^{-1}, pH = 3.4) surrounded by 1,2,4-trimethylbenzene solution containing PS-NH$_2$ (5.0 g L^{-1}) over time (c, 10 s and d, 200 s). (e, f) Confocal fluorescence microscopy images of a water droplet containing H_4TPPS^{2-} (0.4 g L^{-1}, pH = 3.4) surrounded by 1,2,4-trimethylbenzene solution containing PS-*b*-P2VP-*b*-PEO (5.0 g L^{-1}) over time (e, 10 s and f, 200 s). Scale bar; 200 μm.

CONCLUSIONS

In summary, we present an absorption imaging platform to monitor the assembly of SPSs at the water/toluene interface over the entire concentration range. The formation and assembly of SPSs at the interface by the interactions between H_4TPPS^{2-} and mono- and multi-functional ligands, polymer and triblock copolymer, give rise to distinctive color changes that reflect the state of aggregation of the SPSs. Transition between J- and H-aggregates are easily discerned from the color changes that are seen at the interface and in the bulk solutions. An apparent self-wrinkling of the droplet was observed using the interactions between an amphiphilic triblock copolymer, PS-*b*-P2VP-*b*-PEO, dissolved in the toluene and H_4TPPS^{2-} dissolved in water. Due to a crowding of aggregates at the interface. Droplet shapes were seen to change from spherical to oblate ellipsoidal, due to the reduction in the interfacial energy. Our finding proved that adjusting the hydrophilicity and hydrophobicity of the polymer chains

is crucial to the stability of the SPSs at the interface. The time-variant interfaces provide us with more possibilities in synchronizing multifunction and can serve as a sensor to monitor the interfacial behavior of SPSs over the time.

[1]   B. Huang, W. C. Chen, Z. Li, J. Zhang, W. Zhao, Y. Feng, B. Z. Tang, C. S. Lee, *Angew. Chem. Int. Ed.* **2018**, *57*, 12473-12477.
[2]   C. Shahar, S. Dutta, H. Weissman, L. J. Shimon, H. Ott, B. Rybtchinski, *Angew. Chem. Int. Ed.* **2016**, *55*, 179-182.
[3]   R. V. Kazantsev, A. Dannenhoffer, T. Aytun, B. Harutyunyan, D. J. Fairfield, M. J. Bedzyk, S. I. Stupp, *Chem* **2018**, *4*, 1596-1608.
[4]   X. Jia, C. Shao, X. Bai, Q. Zhou, B. Wu, L. Wang, B. Yue, H. Zhu, L. Zhu, *Proc. Natl. Acad. Sci.U S A* **2019**, *116*, 4816-4821.
[5]   S. Kundu, A. Patra, *Chem. Rev.* **2017**, *117*, 712-757.
[6]   K. Liu, C. Yuan, Q. Zou, Z. Xie, X. Yan, *Angew. Chem. Int. Ed.* **2017**, *56*, 7876-7880.
[7]   H. Jiang, L. Zhang, J. Chen, M. Liu, *ACS Nano* **2017**, *11*, 12453-12460.
[8]   N. Zhang, L. Wang, H. Wang, R. Cao, J. Wang, F. Bai, H. Fan, *Nano Lett.* **2018**, *18*, 560-566.
[9]   J. M. Ribó, J. Crusats, J.-A. Farrera, M. L. Valero, *Chem. Commun.* **1994**, 681-682.
[10]   L. Zhao, R. Ma, J. Li, Y. Li, Y. An, L. Shi, *Biomacromolecules* **2008**, *9*, 2601-2608.
[11]   M. A. Castriciano, A. Carbone, A. Saccà, M. G. Donato, N. Micali, A. Romeo, G. De Luca, L. M. Scolaro, *J. Mater. Chem.* **2010**, *20*, 2882.
[12]   G. De Luca, A. Romeo, V. Villari, N. Micali, I. Foltran, E. Foresti, I. G. Lesci, N. Roveri, T. Zuccheri, L. M. Scolaro, *J. Am. Chem. Soc.* **2009**, *131*, 6920-6921.
[13]   N. C. Maiti, M. Ravikanth, S. Mazumdar, N. Periasamy, *J. Phys. Chem.* **1995**, *99*, 17192-17197.
[14]   Y. Egawa, R. Hayashida, J.-i. Anzai, *Langmuir* **2007**, *23*, 13146-13150.
[15]   P. Y. Gu, Y. Chai, H. Hou, G. Xie, Y. Jiang, Q. F. Xu, F. Liu, P. D. Ashby, J. M. Lu, T. P. Russell, *Angew. Chem. Int. Ed.* **2019**, *58*, 12112-12116.
[16]   V. E. Blair, K. Celebi, K. Müllen, J. Vermant, *Adv. Mater. Interfaces* **2019**, *6*, 1801570.
[17]   Z. Niroobakhsh, J. A. LaNasa, A. Belmonte, R. J. Hickey, *Phys. Rev. Lett.* **2019**, *122*, 178003.
[18]   R. M. Clark, K. J. Berean, B. J. Carey, N. Pillai, T. Daeneke, I. S. Cole, K. Latham, K. Kalantar-zadeh, *J. Mater. Chem. C* **2017**, *5*, 6937-6944.
[19]   Y. Zheng, Z. Yu, R. M. Parker, Y. Wu, C. Abell, O. A. Scherman, *Nat. Commun.* **2014**, *5*, 5772.
[20]   G. Luo, Y. Yu, Y. Yuan, X. Chen, Z. Liu, T. Kong, *Adv. Mater.* **2019**, *31*, 1904631.
[21]   B. Qin, S. Zhang, Q. Song, Z. Huang, J. F. Xu, X. Zhang, *Angew. Chem. Int. Ed.* **2017**, *56*, 7639-7643.
[22]   K. Piradashvili, E. M. Alexandrino, F. R. Wurm, K. Landfester, *Chem. Rev.* **2016**, *116*, 2141-2169.

[23] J. F. Neal, W. Zhao, A. J. Grooms, M. A. Smeltzer, B. M. Shook, A. H. Flood, H. C. Allen, *J. Am. Chem. Soc.* **2019**, *141*, 7876-7886.

[24] J. Forth, D. J. French, A. V. Gromov, S. King, S. Titmuss, K. M. Lord, M. J. Ridout, P. J. Wilde, P. S. Clegg, *Langmuir* **2015**, *31*, 9312-9324.

[25] A.-L. Fameau, F. Cousin, L. Navailles, F. Nallet, F. Boué, J.-P. Douliez, *J. Phys. Chem. B* **2011**, *115*, 9033-9039.

[26] Z. Yang, J. Wei, Y. I. Sobolev, B. A. Grzybowski, *Nature* **2018**, *553*, 313.

[27] Y. Chao, H. C. Shum, *Chem. Soc. Rev.* **2020**, *49*, 114-142.

[28] W. Dai, F. Shao, J. Szczerbinski, R. McCaffrey, R. Zenobi, Y. Jin, A. D. Schluter, W. Zhang, *Angew. Chem. Int. Ed.* **2016**, *55*, 213-217.

[29] Y. Zhong, B. Cheng, C. Park, A. Ray, S. Brown, F. Mujid, J.-U. Lee, H. Zhou, J. Suh, K.-H. Lee, *Science* **2019**, *366*, 1379-1384.

[30] M. Nagel, T. A. Tervoort, J. Vermant, *Adv. Coll. Int. Sci.* **2017**, *247*, 33-51.

[31] K. Liu, H. Qi, R. Dong, R. Shivhare, M. Addicoat, T. Zhang, H. Sahabudeen, T. Heine, S. Mannsfeld, U. Kaiser, Z. Zheng, X. Feng, *Nat. Chem.* **2019**, *11*, 994-1000.

[32] H. Sahabudeen, H. Qi, B. A. Glatz, D. Tranca, R. Dong, Y. Hou, T. Zhang, C. Kuttner, T. Lehnert, G. Seifert, U. Kaiser, A. Fery, Z. Zheng, X. Feng, *Nat. Commun.* **2016**, *7*, 13461.

[33] X. Liu, N. Kent, A. Ceballos, R. Streubel, Y. Jiang, Y. Chai, P. Y. Kim, J. Forth, F. Hellman, S. Shi, *Science* **2019**, *365*, 264-267.

[34] H. Q. Peng, X. Zheng, T. Han, R. T. K. Kwok, J. W. Y. Lam, X. Huang, B. Z. Tang, *J. Am. Chem. Soc.* **2017**, *139*, 10150-10156.

[35] X. L. Ni, S. Chen, Y. Yang, Z. Tao, *J. Am. Chem. Soc.* **2016**, *138*, 6177-6183.

[36] Y. Chen, Y. Zhang, D. Karnaushenko, L. Chen, J. Hao, F. Ding, O. G. Schmidt, *Adv. Mater.* **2017**, *29*, 1605165.

[37] J. H. Koo, S. Jeong, H. J. Shim, D. Son, J. Kim, D. C. Kim, S. Choi, J. I. Hong, D. H. Kim, *ACS Nano* **2017**, *11*, 10032-10041.

[38] E. R. Sauve, C. M. Tonge, Z. M. Hudson, *J. Am. Chem. Soc.* **2019**, *141*, 16422-16431.

[39] J. Mei, N. L. Leung, R. T. Kwok, J. W. Lam, B. Z. Tang, *Chem. Rev.* **2015**, *115*, 11718-11940.

[40] Y. Huang, J. Xing, Q. Gong, L.-C. Chen, G. Liu, C. Yao, Z. Wang, H.-L. Zhang, Z. Chen, Q. Zhang, *Nat. Commun.* **2019**, *10*, 169-177.

[41] Y. Huang, Z. Wang, Z. Chen, Q. Zhang, *Angew. Chem. Int. Ed.* **2019**, *58*, 9696-9711.

[42] M. Cui, T. Emrick, T. P. Russell, *Science* **2013**, *342*, 460-463.

[43] J. Forth, P. Y. Kim, G. Xie, X. Liu, B. A. Helms, T. P. Russell, *Adv. Mater.* **2019**, *31*, 1806370.

[44] J. Forth, X. Liu, J. Hasnain, A. Toor, K. Miszta, S. Shi, P. L. Geissler, T. Emrick, B. A. Helms, T. P. Russell, *Adv. Mater.* **2018**, *30*, 1707603.

Entry for the Table of Contents (Please choose one layout)

Layout 1:

COMMUNICATION

Interfacial Interconversion of Porphyrins for the Realization of Color-tunable Structured Liquids: Multicolor structured liquids were prepared by tuning the aggregation of porphyrin. J- and H-aggregates of H_4TPPS^{2-} and H-aggregates of H_2TPPS^4 were formed by electrostatic interaction between H_4TPPS^{2-} and PS-NH$_2$, PS-triNH$_2$, P2VP, and PS-*b*-P2VP-*b*-PEO.
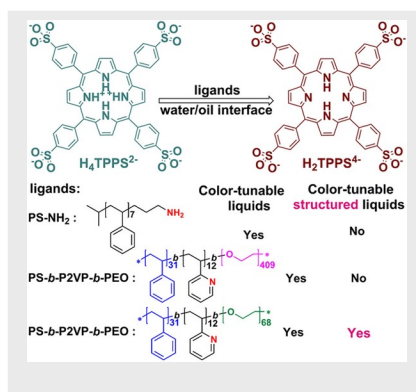
Pei-Yang Gu, Ganhua Xie, Paul Y. Kim, Yu Chai, Xuefei Wu, Yufeng Jiang, Qing-Feng Xu, Feng Liu, Jian-Mei Lu* and Thomas P. Russell*

Page No. – Page No.

Surfactant-induced interfacial aggregation of porphyrins for structuring the color-tunable liquids